JOURNAL OF MATERIALS SCIENCE 5 (1970) 198–217

The Effect of Plastic Bending on the Electrical Properties of Indium Antimonide

Part 2 *Four-Point Bending of n-type Material*

R. L. BELL, A. F. W. WILLOUGHBY
Engineering Materials Laboratory, The University, Southampton, UK

Uniform arrays of In- and Sb-dislocations have been introduced into indium antimonide single crystals by high temperature four-point bending, and the densities of the two types of dislocation estimated by the selective etchants calibrated previously. Hall coefficient and electrical conductivity measurements on bent samples confirm preliminary results that both dislocation types act as acceptor centres in *n*-type material, and interpretations of the temperature-dependence of the electrical properties on the Read and Broudy models have enabled estimation of the dislocation acceptor levels. A new method of analysing experimental data in terms of the Broudy model has been developed, and the model itself modified for the case where the dislocations are in highly polygonised arrays. The different analyses result in widely different dislocation energy levels. From a comparison of these present results with recent studies of dislocations in *p*-type material it is concluded that the unmodified Read model is most appropriate and that the In-dislocation level lies near the centre of the band gap while the Sb-level lies near the valence band.

1. Introduction

In the initial experiment survey described in Part 1 of this investigation [1] three-point bending was used to introduce an excess of either In- or Sb-dislocations [2] into indium antimonide single crystals. Electrical measurements on these samples indicated that both In- and Sb-dislocations act as acceptor centres in *n*-type material, and that In-dislocations act as acceptor centres in *p*-type material. A quantitative analysis was not possible, however, because of the variation of dislocation density between the inner and outer knife edge positions. Subsequently, Bell and Willoughby [3] used four-point bending for etch-pit studies of dislocations in indium antimonide and it was found that a uniform distribution of dislocations could be produced between the inner knife edges. Such a uniform distribution is essential for electrical studies on a macroscopic scale, and specimens bent by this technique have been used to make a detailed study of the electrical properties of dislocations in *n*-type material. The specimens used in this investigation are the same as those used in the previous etch-pit study [3] in which the relative numbers of In- and Sb-dislocations in each specimen were estimated by means of selective etchants calibrated in the first part of that study. The temperature-dependence of the Hall coefficient and conductivity of these specimens, bent to introduce an excess of each type of dislocation, has been used to obtain the energy level of each type of dislocation by means of the theoretical treatments of Read [4] and Broudy [5]. The results are discussed in relation to the previous work reviewed in [1] and to recent investigations of the effects of bending on *p*-type material [6, 7].

2. Experimental Procedure

Single crystals of indium antimonide supplied by the Royal Radar Establishment, Malvern, had an initial electron concentration at 80° K of about 10^{14} cm^{-3} and an etch-pit density of order 10^3 cm^{-2} or less. Specimens were prepared in the form of wafers of dimensions 22 × 10 × 2.5 mm in an orientation to favour single slip during bending. The polarity of the bending direction, i.e. whether In- or Sb-dislocations would be required by the bending, was determined by the etching techniques described elsewhere [3], and

the specimens were deformed in a four-point bending jig at 360° C under a glide strain rate of 5×10^{-6} sec^{-1} at the outer fibre. Full experimental details of the four-point bending technique are given in [3] together with typical stress/strain curves which, as discussed in that reference, indicate that glide occurred on one slip system only. Bar-shaped samples, cut from slices adjacent to the ones used for bending, were used as "control" samples and underwent the heat-treatment given during the bending operation. In certain cases, previously bent material was used for control samples to investigate whether impurity uptake was any greater in material containing a high dislocation density; these are designated "deformed control" samples.

Measurement of the Hall coefficient and electrical conductivity of each bent specimen was made on two samples cut from it in the manner shown in fig. 1. This geometry enables measurement of electrical properties with the current flowing parallel to the expected dislocation direction [8] in one sample, and perpendicular to it in the other. Platinum current leads and potential probes were attached to both these and the control samples by an indium soldering technique [1]; for the samples cut perpendicular to the bend axis the potential probes were attached in the region of uniform dislocation density between the inner knife edges, as shown by the lower two illustrations in fig. 1. A DC technique of Hall coefficient and conductivity measurement was used [1] employing a magnetic field of about 1000 gauss and sample currents of about 200 μA at 80° K and 5 mA at room temperature. Measurements at temperatures intermediate between room temperature and 80°K were obtained by slow-cooling the cryostat with small quantities of liquid nitrogen. After each addition of liquid nitrogen the system was allowed to settle until the maximum temperature variation during the course of a measurement was less than 1° C. For each measurement of conductivity, current reversal was carried out, and for the Hall coefficient field reversal also. The maximum error in the Hall coefficients is estimated as $\pm$ 12% and in the electrical conductivities as $\pm$ 18%.

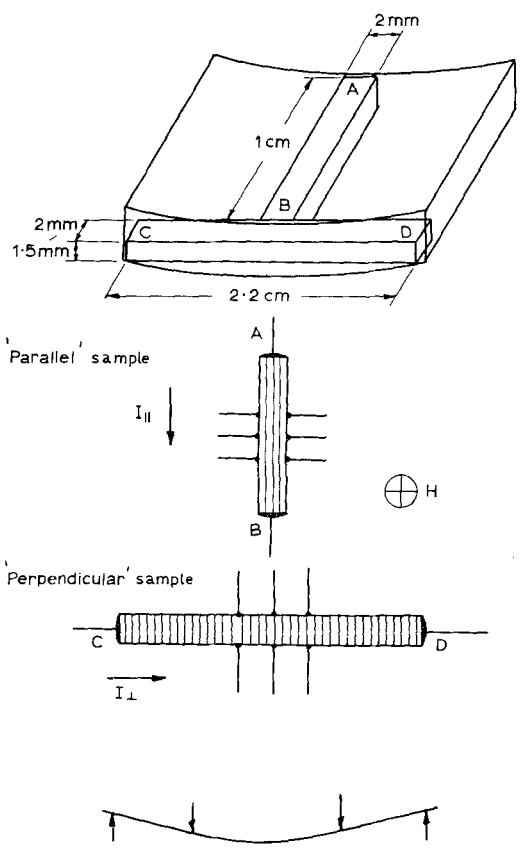

Figure 1 Sectioning of a bent specimen to obtain samples for electrical measurement.

The etch-pit density was measured by sectioning each bent specimen on the octahedral face making an angle of 71° with the bend axis, so that dislocations running parallel to the latter would intersect this face at a steep angle. The two etchants used were modified CP4 and the butylamine etch. Full details of the etching technique and measurements of etch-pit density on the present samples are given in [3].

3. Results

3.1. The Dislocation Distribution in the Bent Samples

It was considered essential to obtain samples with a uniform dislocation density, since the electrical properties of material with a wide variation in dislocation density are extremely complex [5]. For this reason, and also to minimise point-defect production, the bending was performed at a relatively high temperature (360° C) and low strain rate. The etch-pit density of specimens bent by this technique varied by only about 15% in a direction perpendicular to the neutral plane compared with a factor of more than three for specimens bent at 270° C [3]. For positions within the inner knife edges the variation in etch-pit density was also small along directions AB and CD, (fig. 1), being less than

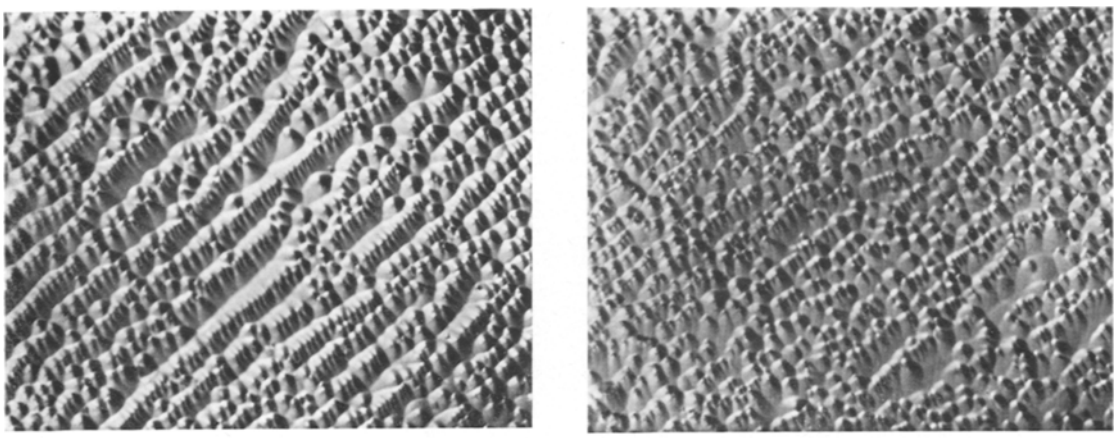

(a) (b)

Figure 2 Etch-pit distribution in (*a*) an In-bent sample (G10); (*b*) an Sb-bent sample (G9). Etchant: Butylamine etch (× 0000).

10% in all cases. This enabled consistent electrical measurements to be made at several points along samples cut parallel to AB and CD. Although the macroscopic etch-pit distribution was very uniform, on a microscopic scale the pits were aligned in polygon walls perpendicular to the slip plane as shown in figs. 2a and b, the alignment being more pronounced in In-bent samples [3].

The densities of In- and Sb-dislocations (ρ_{In} and ρ_{Sb}) in the bent specimens were estimated from the etch-pit densities with the two etchants (ρ_{But} and ρ_{CP_4}) using the following relations [3]:

$$\rho_{But} = \rho_{In} + \rho_{Sb} ;$$
$$\rho_{CP_4} = \rho_{In} + \tfrac{1}{2}\rho_{Sb} .$$

Values of ρ_{In} and ρ_{Sb} calculated in this way for the present specimens are given in [3]. The ratios of majority to minority sign dislocation densities are listed in table I; the values are typically between 3/1 and 4/1 for In-bending and 2/1 and 3/1 for Sb-bending. The reasons for these differing proportions have been discussed previously [3].

It was also considered important to estimate the degree of slip on non-primary systems in the bent samples, since multiple slip would blur the distinction between "parallel" and "perpendicular" samples and would also be likely to produce large numbers of point defects by dislocation interactions. In fact the density of non-primary dislocations, estimated by the etch-pit density on a face cut parallel to the slip plane, was in all cases less than 1% of the density of primary dislocations.

3.2. Hall Coefficient and Electrical Conductivity Measurements

3.2.1. The effect of Heat-treatment on the Control Samples

The control samples, both undeformed and deformed, were measured before and after the heat-treatment, and in no sample was any significant change in either the Hall coefficient or the conductivity detected. It is therefore concluded that impurity uptake during heat-treatment at 360° C was insignificant, even in samples containing a high dislocation density.

3.2.2. Measurements on Bent and Control Samples over the Range 80 to 300° K

In the case of two In-bent and two Sb-bent specimens the Hall coefficients of both control and deformed samples were measured over the temperature range 80 to 300° K; the results are plotted in fig. 3. In all cases the values of $R_{\parallel}$ and $R_{\perp}$ for corresponding samples were equal, within experimental error, and so only $R_{\parallel}$ is plotted in the figure. (The subscripts $\parallel$, $\perp$ and 0 refer to the parallel, perpendicular and control samples respectively.)

In the intrinsic range the Hall coefficient curves for control and deformed samples are superimposed. Throughout the extrinsic range, however, the Hall coefficient of deformed samples is greater than that of the control samples for both Sb- and In-bending which appears to indicate the introduction of acceptors in the two cases. In the extrinsic range, the control

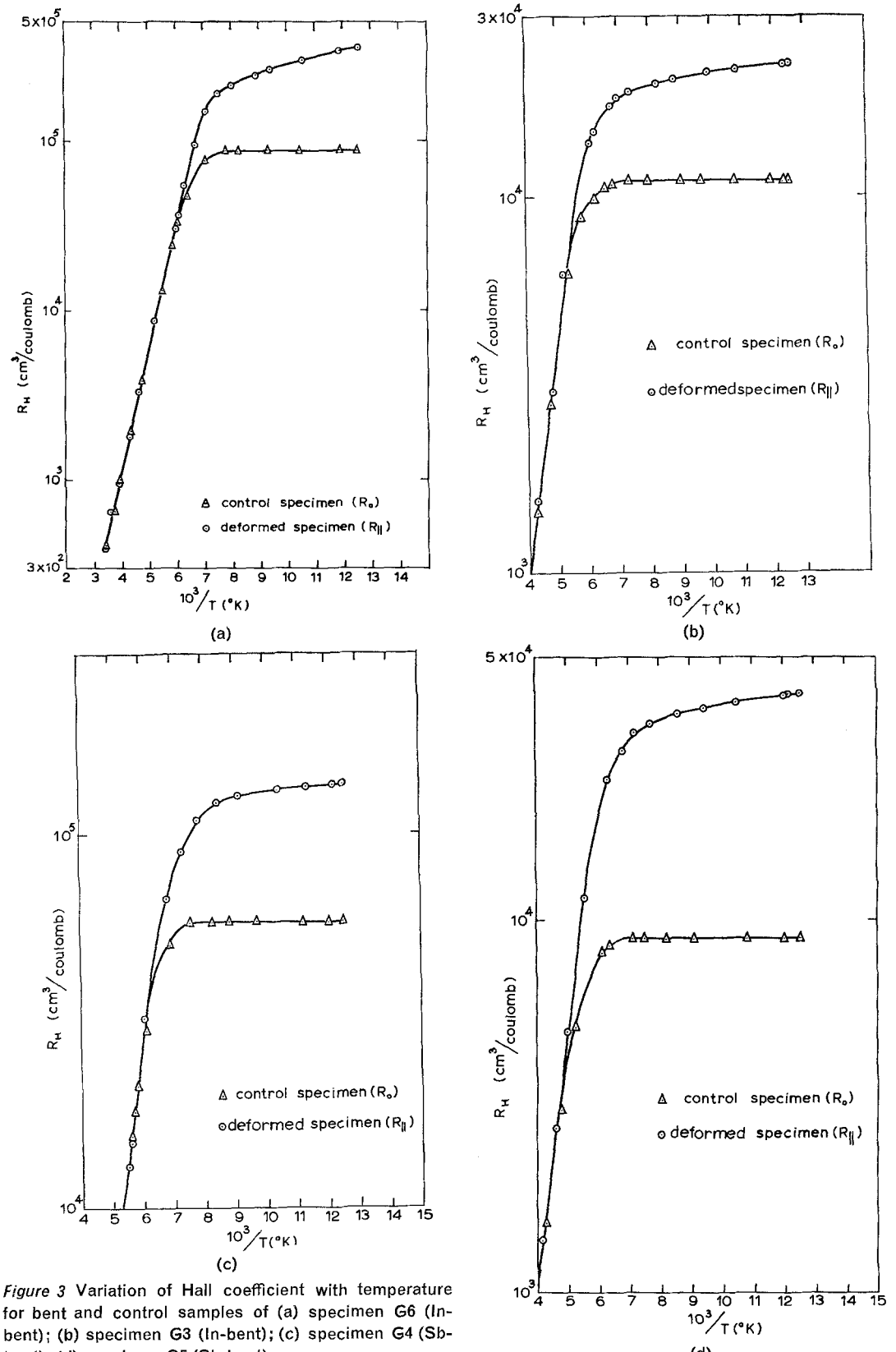

Figure 3 Variation of Hall coefficient with temperature for bent and control samples of (a) specimen G6 (In-bent); (b) specimen G3 (In-bent); (c) specimen G4 (Sb-bent); (d) specimen G5 (Sb-bent).

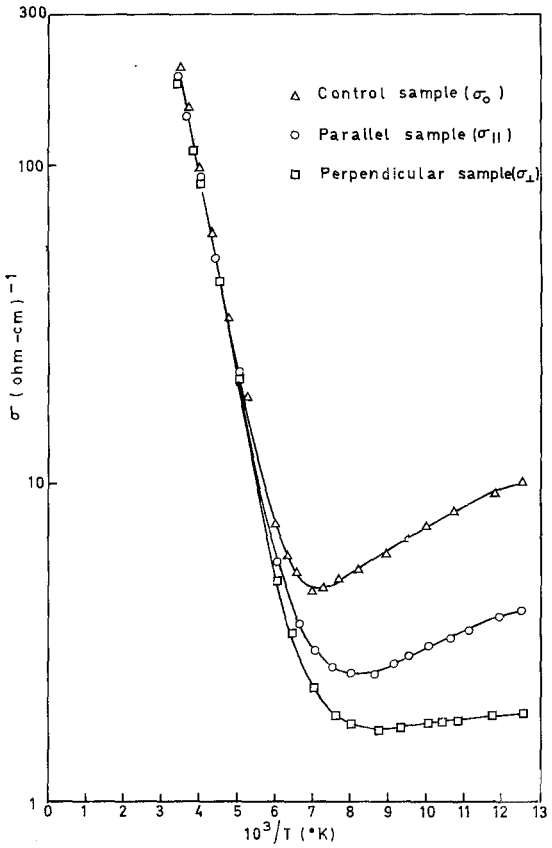

Figure 4 Variation of electrical conductivity with temperature for bent and control samples of specimen G4 (Sb-bent).

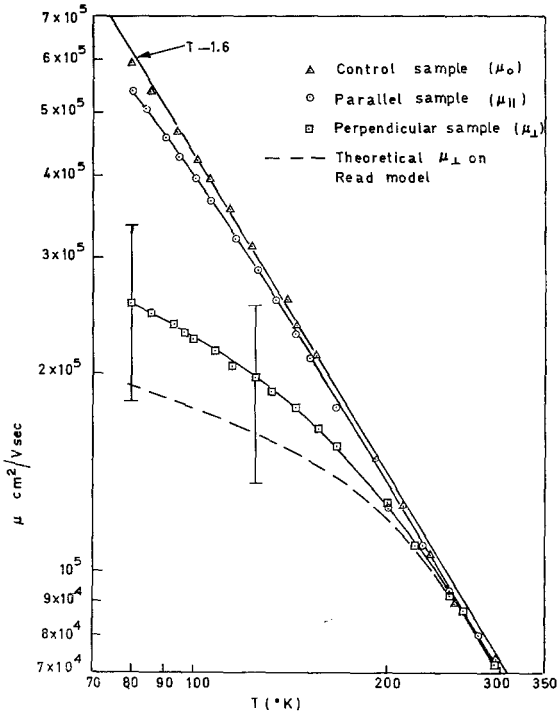

Figure 5 The variation of Hall mobility with temperature for bent and control samples of specimens G4 (Sb-bent) compared with a curve of $\mu_{\perp}$ calculated on the Read model.

samples have a temperature-independent Hall coefficient which is characteristic of ordinary n-type material [9], while that of the deformed samples increases as the temperature falls as in the freeze-out of impurity centres. The slopes, however, are too shallow for any known impurity level and in sections 4 and 5 the results are analysed in terms of models of dislocation acceptors which, because of the electrostatic interaction between the accepted electrons along a dislocation line, predict an entirely different temperature-dependence of the Hall coefficient.

Fig. 4 shows the temperature-dependence of the electrical conductivity of the Sb-bent specimen G4, and compares the curves for control, parallel and perpendicular samples. The Hall mobility $\mu(= R\sigma)$ is plotted in fig. 5 for the same samples and shows that, below about 200° K the three curves diverge such that $\mu_0 > \mu_{\parallel} > \mu_{\perp}$ until at 80° K $\mu_{\perp}/\mu_0 = 0.3$ and $\mu_{\parallel}/\mu_0 = 0.8$. This behaviour is typical of both In- and Sb-bent specimens (see section 3.2.3 and table II). Such an anisotropic mobility in the deformed specimens would be expected [4] if dislocations lie mainly along the bend axis, but Read's theory predicts that the mobility in the parallel samples should be unchanged as compared with the control samples. The temperature-dependence of the Hall mobility of the control samples obeys the relation $\mu \alpha T^{-1.6}$ found by Putley [9] and explained by Ehrenreich [10] in terms of combined optical phonon and electron-hole scattering, but below 200° K the behaviour of the deformed samples indicates the presence of another scattering mechanism. In section 4.3 this will be analysed in terms of the effect of dislocations on mobility.

3.2.3. *Samples Bent to a Variety of Radii and Measured at 300 and 80° K*

Measurements were made at two fixed temperatures, 300 and 80° K, on a large number of samples which had been bent to a variety of radii from 2.5 to 50 cm. At 300° K the Hall coefficient and conductivity of each sample was equal to the intrinsic value as observed in section 3.2.2. The

TABLE I Hall coefficient and conductivity measurements at 80°K on undeformed control samples (R_0, σ_0), parallel samples ($R_{\parallel}$, $\sigma_{\parallel}$) and perpendicular samples ($R_{\perp}$, $\sigma_{\perp}$), and their etch-pit densities (ρ_{But})

In-bent specimens

Spec. no.	ρ_{But}, cm^{-2}	ρ_{In}/ρ_{Sb}	R_0 (*n*-type), cm^3/Coul	$R_{\perp} = R_{\parallel}$ (*n*-type), cm^3/Coul	σ_0, cm^{-1}	$\sigma_{\parallel}$, Ω-cm^{-1}	$\sigma_{\perp}$, Ω-cm^{-1}
G11	7.25×10^5	2.76	7.45×10^4	7.84×10^4	7.58	6.79	6.15
G1	1.4×10^6	3.67	6.61×10^4	7.38×10^4	8.58	7.59	6.05
G12	2.88×10^6	2.79	8.82×10^4	1.23×10^5	5.33	3.51	2.52
G2	3.18×10^6	3.05	1.34×10^5	3.05×10^5	3.55	1.43	0.639
G6	5.82×10^6	3.7	8.80×10^4	3.56×10^5	6.36	1.38	0.44
G10	1.35×10^7	3.5	5.3×10^4	2.74×10^5	9.56	1.15	0.42
G3	3.30×10^7	3.12	1.1×10^4	2.25×10^4	38.2	17.19	5.97
	ρ_{But}		R_0 (*n*-type)	$R_{\perp}$ (*p*-type)	σ_0 (*n*-type)		$\sigma_{\perp}$ (*p*-type)
G15	2.67×10^7		7.50×10^4	5.21×10^4	7.60		0.112

Sb-bent specimens

Spec. no.	ρ_{But}	ρ_{Sb}/ρ_{In}	R_0 (*n*-type)	$R_{\perp} = R_{\parallel}$ (*n*-type)	σ_0 (*n*-type)	$\sigma_{\parallel}$ (*n*-type)	$\sigma_{\perp}$ (*n*-type)
G4	1.71×10^6	2.42	5.81×10^4	1.35×10^5	10.2	3.98	1.88
G7	2.02×10^6	2.48	4.28×10^4	7.27×10^4	12.3	6.22	3.08
G8	3.1×10^6	2.45	3.36×10^4	6.945×10^4	16.55	6.70	2.88
G13	5.05×10^6	2.43	1.04×10^4	1.427×10^4	37.8	24.8	15.56
G14	7.27×10^6	2.48	8.62×10^3	1.147×10^4	47.9	32.6	20.05
G9	9.6×10^6	2.48	6.65×10^3	8.954×10^3	52.34	35.0	22.34
G5	1.45×10^7	3.14	9.00×10^3	3.99×10^4	45.6	8.16	2.44

measurements at 80° K are given in table I together with the etch-pit density obtained with the butylamine etch (ρ_{But}). One In-bent sample (Number G15) was converted to *p*-type by the bending.

In general, for samples remaining *n*-type after bending, the results given in table I confirm the trends found in section 3.2.2., i.e. $R_{\parallel} = R_{\perp} > R_0$ and $\mu_0 > \mu_{\parallel} > \mu_{\perp}$, for both Sb- and In-bending. All the results, including those from specimen G15, indicate that both In- and Sb-bending introduce acceptor centres and reduce the mobility to a greater extent in the perpendicular samples than in the parallel ones.

4. Analysis of Results on the Read Model of Dislocation Acceptors

Since all the measurements detailed above are consistent with the idea of deformation-induced acceptors, it seems reasonable to analyse the measurements quantitatively in terms of a model such as that postulated by Read [4] for dislocations in germanium. On this model the dislocation acceptor centres have a single level within the energy gap but the occupation statistics are limited by the increase in electrostatic energy of the system so that the fraction, f, of sites occupied is given on the "minimum energy" approximation, by the expression

$$(E_C - E_D) - (E_C - E_F) = E_0 f\{3\ln f/f_c - 0.232\} \quad (1)$$

where, measuring energies from the top of the valence band, E_D is the dislocation energy level at the dislocation, E_F is the Fermi level in normal material, E_C is the conduction band energy, $E_0 = q^2/\kappa c$, $f_c = c\pi^{1/3}(N_D - N_A)^{1/3}$ and c = spacing of dangling bonds = $0.866b$ cosec α where α = angle between dislocation line and its Burgers vector. On the "Fermi" approximation, which allows non-uniform spacing of electrons along the dislocation but assumes that all configurations have the same energy, the appropriate expression is

$$(E_C - E_D) - (E_C - E_F) + kT\ln\left(\frac{1-f}{f}\right) = E_0 f\{3\ln f/f_c - 0.232\} \quad (2)$$

The Read model has been modified for the case of the sphalerite structure by Gatos and Lavine [11] and Holt [12], both of whom suggest that each type of dislocation is associated with

more than one level. To simplify the analysis, however, it will be assumed here that there is just the one energy level associated with each of the two types of dislocation. It will be further assumed that the dislocations in all samples were predominantly of the pure edge type.

4.1. Analysis of Hall Coefficient Measurements on Samples Bent to Various Radii

In order to interpret electrical measurements on material containing dislocations Read [4] and subsequently Logan *et al* [13] and Broudy [5] have made theoretical treatments of conduction in material containing a parallel array of dislocation space charge cylinders. Assuming that specular scattering of electrons occurs at the surface of these cylinders, Read [4] and Logan *et al* [13] obtained the following expression for $R_\perp$ in terms of $\langle n \rangle$, the average carrier concentration in the perpendicular sample

$$R_\perp = \frac{\mu_H}{\mu \langle n \rangle q} \qquad (3)$$

where μ_H is the Hall, and μ the drift mobility. Logan *et al* [13] and Broudy [5] obtained the same expression for $R_\parallel$. The present measurements all confirm the prediction that $R_\parallel = R_\perp$ and equation 3 has therefore been used to calculate $\langle n \rangle$ at 80° K, from the data of table I. (In the case of the *p*-type sample a similar relation has been used to calculate $\langle p \rangle$.) These values are given in table II together with values of n, the carrier concentration in the control samples; $\mu_H/\mu = 1$ has been assumed throughout.

Values of the net change in carrier concentration, $(n - \langle n \rangle)$ or $(n + \langle p \rangle)$, are given in this table, and are plotted against the etch-pit density, ρ_{But}, in fig. 6, together with corresponding results from the three-point bending investigation [1]. Within experimental error the results for Sb-bent samples lie on a straight line of slope $= 3.85 \times 10^7$ cm^{-1} while those for the In-bent samples lie on a line of slope $= 0.816 \times 10^7$ cm^{-1}. Now on Read's theory the change in carrier concentration at a given temperature due to the introduction of ρ dislocations per cm^2 is given by the expression

$$\epsilon = \frac{n - \langle n \rangle}{n} = \frac{f\rho}{cn} \qquad (4)$$

(where ϵ is the fraction of material in the space charge cylinders), and thus, if f is constant*,

TABLE II Read interpretation of measurements at 80° K

In-bent specimens

Spec. no.	ρ_{But}, cm^{-2}	n, cm^{-3}	$\langle n \rangle$, cm^{-3}	$n - \langle n \rangle$, cm^{-3}	μ_0, cm^2/Vsec	$\mu_\parallel$, cm^2/V sec	$\mu_\perp$, cm^2/V sec
G11	7.25×10^5	8.39×10^{13}	7.97×10^{13}	0.42×10^{13}	5.65×10^5	5.32×10^5	4.82×10^5
G1	1.4×10^6	9.45×10^{13}	8.47×10^{13}	0.98×10^{13}	5.67×10^5	5.60×10^5	4.47×10^5
G12	2.88×10^6	7.09×10^{13}	5.08×10^{13}	2.01×10^{13}	4.70×10^5	4.32×10^5	3.10×10^5
G2	3.18×10^6	4.66×10^{13}	2.61×10^{13}	2.05×10^{13}	4.76×10^5	4.37×10^5	1.95×10^5
G6	5.82×10^6	7.11×10^{13}	1.75×10^{13}	5.36×10^{13}	5.6×10^5	4.92×10^5	1.58×10^5
G10	1.35×10^7	1.18×10^{14}	2.28×10^{13}	9.52×10^{13}	5.07×10^5	3.15×10^5	1.15×10^5
G3	3.30×10^7	5.68×10^{14}	2.78×10^{14}	2.90×10^{14}	4.2×10^5	3.88×10^5	1.34×10^5
	ρ_{But}, cm^{-2}	n, cm^{-3}	$\langle p \rangle$, cm^{-3}	$n + \langle p \rangle$, cm^{-3}	μ_0 (n-type), cm^2/V sec		μ (p-type), cm^2/V sec
G15	2.67×10^7	8.33×10^{13}	1.20×10^{14}	2.03×10^{14}	5.7×10^5		5.83×10^3

Sb-bent specimens

Spec. no.	ρ_{But}	n	$\langle n \rangle$	$n - \langle n \rangle$	μ_0	$\mu_\parallel$	$\mu_\perp$
G4	1.71×10^6	1.075×10^{14}	4.63×10^{13}	6.12×10^{13}	5.9×10^5	5.37×10^5	2.55×10^5
G7	2.02×10^6	1.46×10^{14}	8.60×10^{13}	6.0×10^{13}	5.26×10^5	4.52×10^5	2.24×10^5
G8	3.1×10^6	1.86×10^{14}	9.00×10^{13}	9.6×10^{13}	5.56×10^5	4.65×10^5	2.00×10^5
G13	5.05×10^6	6.00×10^{14}	4.38×10^{14}	1.62×10^{14}	3.93×10^5	3.54×10^5	2.22×10^5
G14	7.27×10^6	7.25×10^{14}	5.45×10^{14}	1.80×10^{14}	4.13×10^5	3.74×10^5	2.3×10^5
G9	9.6×10^6	9.40×10^{14}	6.98×10^{14}	2.42×10^{14}	3.48×10^5	3.13×10^5	2.0×10^5
G5	1.45×10^7	6.94×10^{14}	1.57×10^{14}	5.37×10^{14}	4.1×10^5	3.26×10^5	0.972×10^5

*In fact f is not expected to be exactly the same for each sample since the carrier concentration, and E_F, of each was different initially, but this is likely to give a variation of f values of only about $\pm 10\%$ as shown for each value of dislocation energy level in table IV.

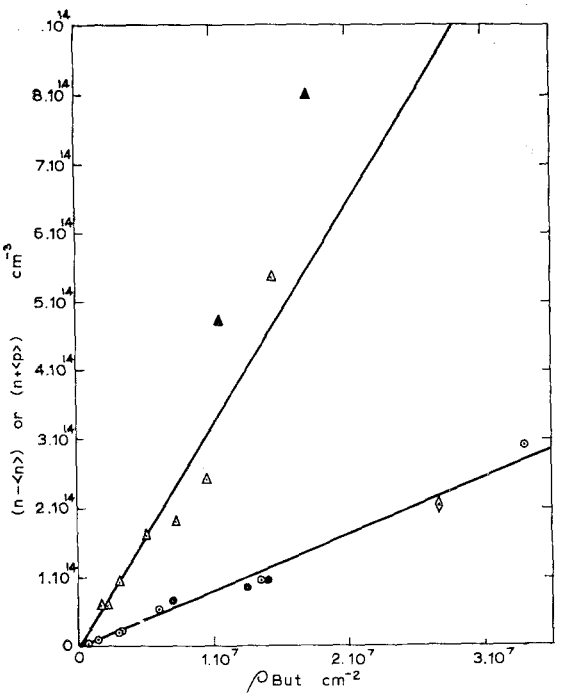

Figure 6 Increase in acceptor concentration after bending, measured at 80° K, versus etch-pit density in In-bent and Sb-bent specimens. Those remaining *n*-type after bending are shown as: △, Sb-bent; ○, In-bent; ●, In-bent, (from previous investigation [1] employing 3-point bending). Those converted to *p*-type by the bending are shown as: ◈, In-bent; ▲, Sb-bent (from previous investigation [1]).
The straight lines are drawn giving least weight to the three-point bent samples because of difficulties associated with the non-uniform dislocation distribution in these.

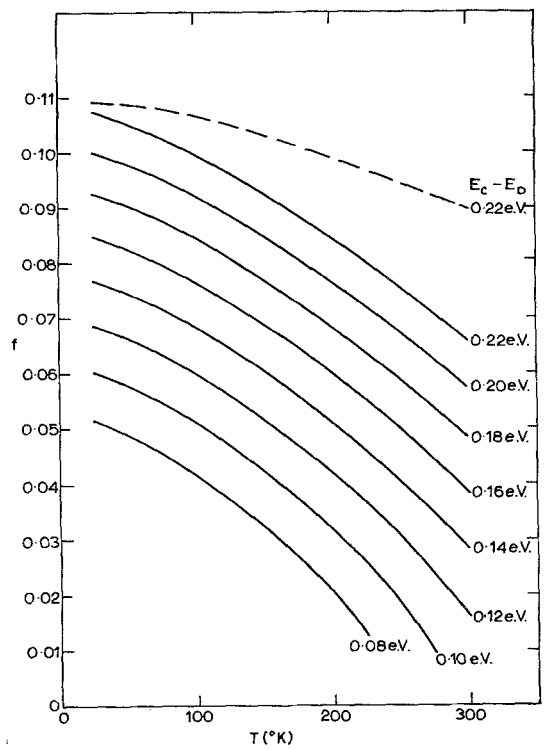

Figure 7 Variation of *f*, the fraction of dislocation acceptors occupied, with temperature for various values of the dislocation energy level ($E_C - E_D$). Continuous lines calculated by Read's "minimum energy" approximation, and broken line by the "Fermi" approximation.

$n - \langle n\rangle$ should be directly proportional to ρ as observed. The difference between the slopes for Sb-bent and In-bent specimens indicates that Sb-dislocations provide more than four times the number of acceptor centres per unit length than do the In-dislocations and suggests that the Sb-dislocation level is lower in the forbidden gap than the In-level. The systematic dependence of acceptor concentration on dislocation density shown in fig. 6 provides good evidence that the acceptors are associated with dislocations rather than with another species of deformation induced defect.

4.2. Analysis of Temperature-Dependence of the Hall Coefficient of Bent Samples and Calculation of Dislocation Energy Levels

For each specimen it was first necessary to calculate the position of the Fermi level in the undeformed material. The expression used for this was

$$E_C - E_F = kT \ln \left\{ \frac{2(2\pi m^* kT/h^2)^{3/2}}{(N_D - N_A)} \right\},$$

and, with the values $c = 4$ Å, $\kappa = 16$, and $m^* = 0.013\, m_0$, equation 1, which is an implicit function of f, was then solved by a numerical method for several selected values of $(E_C - E_D)$ so as to give a family of f versus temperature curves such as that shown in fig. 7. One of these curves, say the one for $(E_C - E_D) = 0.08$ eV, was then selected for the first comparison with experimental results. Following the method of Logan *et al* [13] relation 4 was re-written in the form

$$\epsilon(T) = \lambda f(T) \tag{5}$$

where

$$\lambda = \frac{\rho}{c(N_D - N_A)} \tag{6}$$

Values of $\epsilon(T)$, obtained directly from the experimental results by the relation

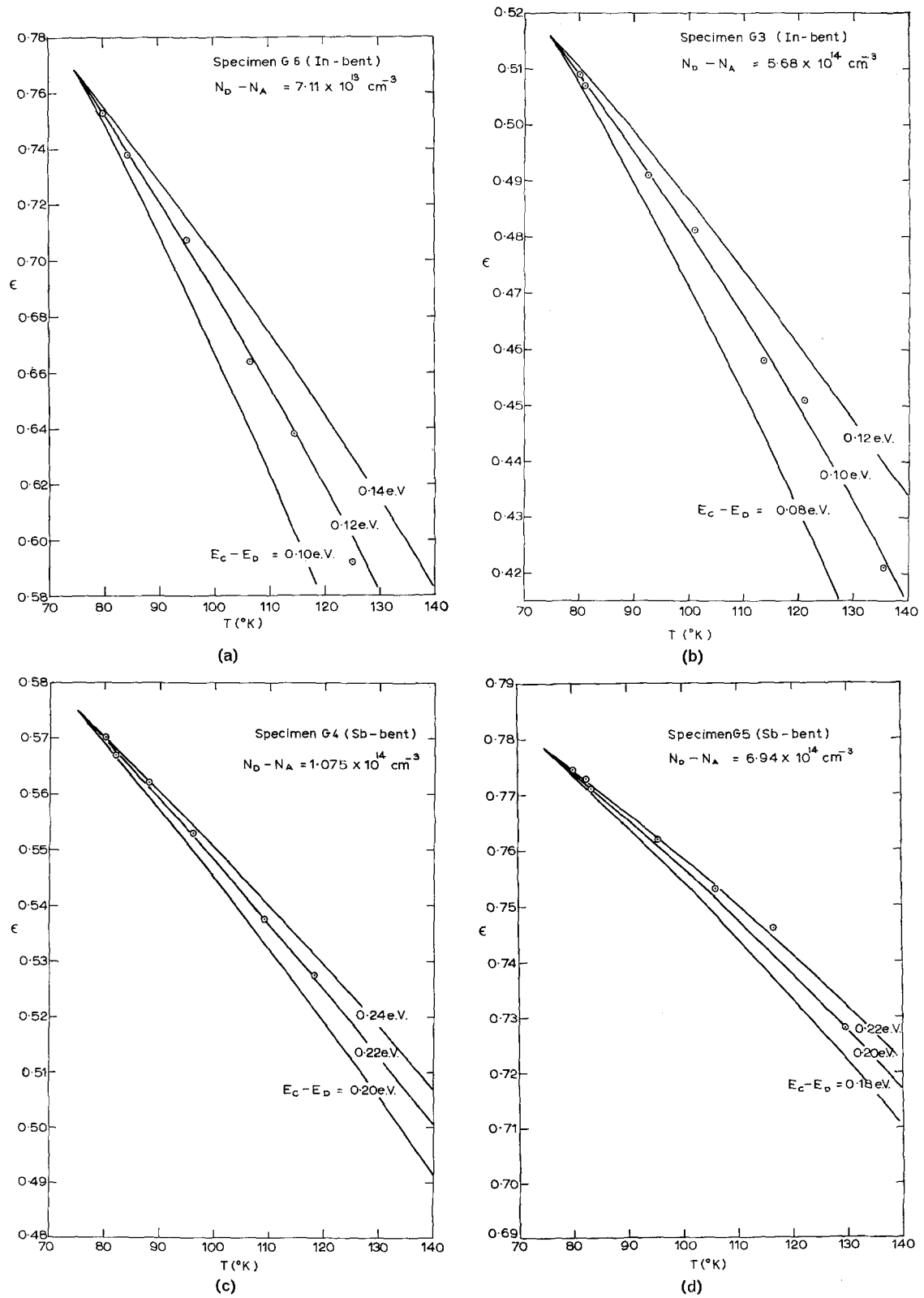

Figure 8 Experimental values of $\epsilon(= 1 - R_0/R_{\parallel})$, plotted against temperature, compared with curves calculated on the Read model for various values of the dislocation energy level.

$\epsilon = 1 - (R_0/R_{\parallel})$, were plotted as experimental points, e.g. fig. 8a and by fitting the theoretical f versus T curve at one temperature (75° K) the value of λ was obtained. This value was then used to convert the theoretical f versus T curve into that for ϵ versus T. The procedure was repeated for f versus T curves apertaining to other values of $(E_C - E_D)$ and it was seen that $E_C - E_D = 0.12$ eV gave the best fit over the range of temperature. From the value of λ used, the dislocation density was derived from equation 6.

The observed temperature-dependence of the Hall coefficient of all samples measured could be accommodated in this way using $f(T)$ curves calculated by Read's "minimum energy" approximation but not by those obtained on the "Fermi" approximation. The quality of the fits obtained with curves based on the "minimum energy approximation" is shown in fig. 8, while the acceptor levels and dislocation densities deduced are listed in table III together with the measured etch-pit densities. The analysis places the In-dislocation level near the centre of the gap and the Sb-level close to the valence band, fig. 9.

Comparing the measured etch-pit densities with the dislocation densities deduced from the above analysis there is a discrepancy of a factor of about seven for In-bending and fifteen for Sb-bending. These two different factors are confirmed approximately by the data in table IV which relates to specimens whose electrical properties were measured only at two fixed temperatures. Here f-values were calculated on the basis of the $(E_C - E_D)$-values deduced above. It will be noted that in all cases comparison is being made with the dislocation density given by the butylamine etch which reveals not just the majority dislocations but the total dislocation content [3]. Had the comparison been with the number of majority sign dislocations only, the discrepancies would have been worse. In view of

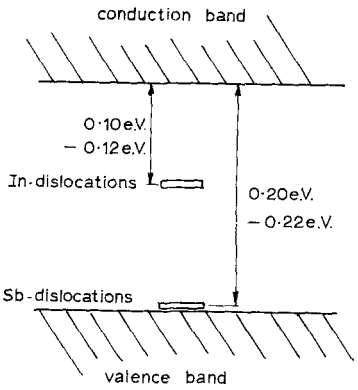

Figure 9 Scheme of dislocation acceptor levels resulting from Read analysis.

previous work on the efficiency of etching dislocations in material with the diamond or sphalerite structure [3, 14], the large overestimates given by the analysis based on the Read model are considered to be a major shortcoming of the application of it to InSb.

4.3. Analysis of Hall Mobility Measurements

Read [4] assumed that specular scattering of electrons occurred at the surface of the space charge cylinders and thus considered that scattering by dislocations would have a negligible effect on mobility for current flow parallel to the space charge tubes. This prediction is not well confirmed by the present results, for, although most of the $\mu_{\parallel}$ values in table II are within experimental error of corresponding values of μ_0, $\mu_{\parallel}$ was in all cases less than μ_0. For current flow normal to the dislocations Read suggested that the mobility would be reduced both by distortion of the current streamlines and by scattering at space charge cylinders, and Logan *et al* [13] developed this model to obtain

$$\frac{\mu_{\perp}}{\mu_0} = g(\epsilon)\, F(X) \qquad (7)$$

TABLE III Read Interpretation

Spec. no.	Excess dislocation type	E_C-E_D, eV	Dislocation density, cm^{-2}		$\mu_{\perp}$, cm^2/V sec		$\frac{\mu_{\perp}\text{ (calculated)}}{\mu_{\perp}\text{ (experimental)}}$
			Calculated	Etch-pit (ρ_{But})	Calculated	Experimental	
G6	In	0.12	4.49×10^7	5.82×10^6	1.24×10^5	1.58×10^5	0.785
G3	In	0.10	2.14×10^8	3.30×10^7	0.966×10^5	1.34×10^5	0.721
G4	Sb	0.22	2.86×10^7	1.71×10^6	1.89×10^5	2.55×10^5	0.741
G5	Sb	0.20 – 0.22	2.06×10^8	1.45×10^7	0.644×10^5	0.972×10^5	0.662

where $g(\epsilon)$ is a distortion parameter obtained empirically by Morgan [4] and theoretically by Juretschke *et al* [15]. $F(X)$ represents the reduction in mobility by scattering, where $X = l/l_D$, l is the mean free path in undeformed material in which acoustic scattering was assumed to predominate, and l_D is the mean free path for dislocation scattering which is given by the following relation derived by Logan *et al*

$$l_D = \frac{3}{8R_s\rho} \tag{8}$$

where R_s, the radius of the space charge tubes, was given by Read as

$$R_s = \left[\frac{f}{\pi c(N_D - N_A)}\right]^{\frac{1}{2}} \tag{9}$$

Duga [16] subsequently modified this treatment for the case of indium antimonide where impurity scattering may be a significant scattering mechanism at 80° K, and obtained

$$\mu_\perp = \mu_A g(\epsilon)\, F(X)\, K(\beta^*) \tag{10}$$

where μ_A is the mobility (in an undeformed sample) limited only by acoustic scattering, and the additional term $K(\beta^*)$ represents the effect of impurity scattering in the deformed sample.

It must be noted at this stage that Duga's calculation was based on the assumption that scattering by acoustic phonons is the dominant lattice scattering mechanism in InSb, while Ehrenreich [10] has shown that polar scattering is dominant over the acoustic modes at higher temperatures and probably also at 80° K. It is possible, therefore, that Duga's treatment is incorrect, but, in the absence of any comparable treatment using polar scattering, the present results have been analysed on the Duga theory bearing in mind this objection.

Values of $\mu_\perp$, to compare with experimental measurements listed above, were calculated from equation 10 in which the constituent parameters were obtained as follows: β, the degree of impurity scattering in the undeformed material, was calculated from the temperature-dependence of the Hall mobility of the control samples, by the method of Bate, Willardson, and Beer [17] which uses the relation $\mu_0 = \mu_A K(\beta)$. For sample G4, $K(\beta) \to 1$ at all temperatures and thus throughout the following calculations μ_A was taken as the measured mobility of this control sample. The calculation of ϵ from the Hall coefficient measurements was detailed above, and $g(\epsilon)$ was interpolated from the graph of Read [4]. The mean free path for acoustic scattering, l_A, was calculated from μ_A by the classical expression

$$l_A = \frac{3\mu_A}{4q}(2\pi m^* kT)^{\frac{1}{2}},$$

derived by Wilson [18], and l_D was obtained from equation 8 using the value of ρ resulting from the analysis of the Hall coefficient measurements (section 4.2). After calculating $X = l_A/l_D$

TABLE IV Read interpretation: comparison of theory and experiment. Theoretical values calculated assuming $E_C - E_D = 0.12$ eV for In-dislocations and 0.20 eV for Sb-dislocations

In-bent specimens Spec. no.	$f(80°\text{ K})$ $E_C - E_D =$ 0.12 eV	ρ_{theor}, cm^{-2} (from R_H)	ρ_{But}, cm^{-2}	$\frac{\rho_{theor}}{\rho_{But}}$	$\mu_\perp$(calc), cm^2/V sec	$\mu_\perp$(expt), cm^2/V sec	$\frac{\mu_\perp \text{ (calc)}}{\mu_\perp \text{ (expt)}}$
G11	0.0477	3.523×10^6	7.25×10^5	4.87	4.93×10^5	4.82×10^5	1.02
G1	0.0486	8.067×10^6	1.4×10^6	5.75	4.02×10^5	4.47×10^5	0.899
G12	0.0466	1.726×10^7	2.88×10^6	6.00	2.37×10^5	3.10×10^5	0.764
G2	0.0439	1.868×10^7	3.18×10^6	5.88	1.57×10^5	1.95×10^5	0.805
G10	0.0502	7.585×10^7	1.35×10^7	5.62	0.78×10^5	1.15×10^5	0.678
Sb-bent specimens Spec. no.	$f(80°\text{ K})$ $E_C - E_D =$ 0.20 eV	ρ_{theor}, cm^{-2} (from R_H)	ρ_{But}, cm^{-2}	$\frac{\rho_{theor}}{\rho_{But}}$	$\mu_\perp$ (calc), cm^2/V sec	$\mu_\perp$ (expt), cm^2/V sec	$\frac{\mu_\perp \text{ (calc)}}{\mu_\perp \text{ (expt)}}$
G7	0.0815	2.945×10^7	2.02×10^6	14.6	1.77×10^5	2.24×10^5	0.79
G8	0.0836	4.594×10^7	3.1×10^6	14.8	1.38×10^5	2.00×10^5	0.69
G13	0.0954	6.793×10^7	5.05×10^6	13.4	1.60×10^5	2.22×10^5	0.721
G14	0.0974	7.393×10^7	7.27×10^6	10.4	1.69×10^5	2.3×10^5	0.735
G9	0.1004	9.642×10^7	9.6×10^6	10.0	1.44×10^5	2.0×10^5	0.72

the function $F(X)$ was interpolated from the graph of Logan *et al* [13].

β^* was calculated from the expression

$$\beta^* = \frac{2Q\beta \sec \alpha}{\pi \quad X} \log \left[\frac{\sin \alpha/2}{\cos(-\alpha/2)}\right], \quad (11)$$

where $\alpha = \sin^{-1}(1/X)$, and the value of Q was obtained from the Hall coefficient measurements using Duga's expressions [16]. $K(\beta^*)$ was then obtained by interpolation from the tabulated values of Beer *et al* [19].

Values of $\mu_\perp$ computed by the above method are compared in table III with the experimental values. The computed values are consistently less than the experimental ones by about 30%; this is within experimental error but such a trend is to be expected if the dislocations do not all lie parallel to the bend axis; this would also explain the observation that $\mu_\parallel < \mu_0$. Fig. 5 compares the dependence on temperature of the computed and experimental mobilities of sample G4, and shows that the two curves agree within experimental error over the whole range of temperature.

Values of $\mu_\perp$ have also been calculated using equation 7 for samples bent to a range of radii and measured at the one temperature, 80° K, using the dislocation density computed previously. Table IV compares these values with the experimental ones and confirms the trends found in the samples investigated more extensively. The errors produced by using equation 7, i.e. assuming that impurity scattering is negligible, can be estimated from a similar computation of $\mu_\perp$ for sample G5, which results in a value of 0.590×10^5 cm²/V sec via equation 7, compared with 0.644×10^5 cm²/V sec via equation 10, an error of about 8.4%. The discrepancy for the other samples is expected to be even smaller since sample G5 was one of the most heavily doped samples used.

5. Analysis of Measurements on the Broudy Non-Specular Scattering Model

Some of the apparent inconsistencies of the present results with the predictions of the Read model, viz. the observed reduction in electron mobility parallel to the dislocations, and the need to assume a large under-estimation of dislocation density by the etch-pit technique, can be avoided by adopting the modification suggested by Broudy [5] for the analysis of his own results on deformed germanium, that the reflection of electrons at the dislocation space charge tubes is non-specular. The electron mobility (μ_2) in the region within one mean free path (ℓ) of the space charge tubes (the ϕ-region) is then effectively lower than the mobility (μ_1) in the region further away, as illustrated in fig. 10. For current flow

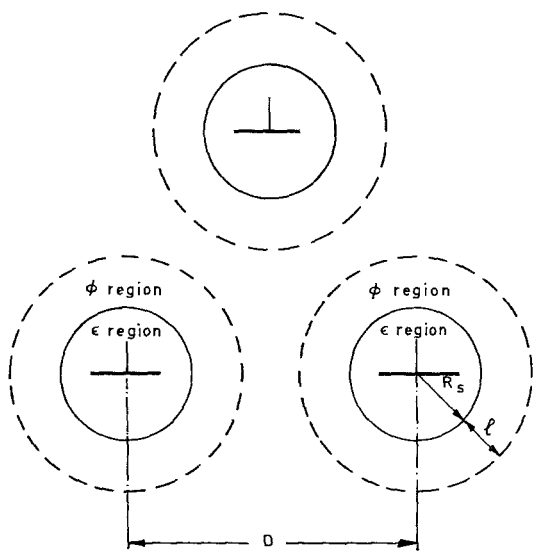

Figure 10 The Broudy model. R_S, radius of the space charge cylinders, ℓ, mean free path of electrons, D, distance between dislocations.

parallel to the dislocations the material is then approximately equivalent to a system of two sets of parallel conductors with a third set of parallel insulating cores. Using the following simple formulae for the conductivity and Hall coefficient of a composite of two parallel conductors of conductivities σ_1 and σ_2, electron mobilities μ_1 and μ_2, and carrier concentrations n_1 and n_2,

$$R = \frac{(1+B)\,[1 + (B\mu_1\sigma_1/\mu_2\sigma_2)]}{n_2 q[1 + (B\sigma_1/\sigma_2)]^2}; \quad (12)$$

$$\sigma = \frac{(\sigma_2 + B\sigma_1)}{(1+B)}; \quad (13)$$

where B is the ratio of the cross-sectional areas of the conductors 1 and 2, Broudy obtained the following relations for the Hall coefficient and conductivity of the three region arrangement:

$$R_\parallel/R_0 = \frac{1 - \epsilon - (1-\theta^2)\phi}{[1 - \epsilon - (1-\theta)\phi]^2}, \quad (14)$$

$$\sigma_\parallel/\sigma_0 = 1 - \epsilon - (1-\theta)\phi, \quad (15)$$

and

$$\sigma_\perp/\sigma_\parallel = \frac{1}{[1 + \epsilon + \phi(1-\theta)]}, \quad (16)$$

where $\theta = \mu_2/\mu_1$, ϵ = fraction of material in space charge tubes (as in Read model), and

$$\phi = \rho\pi(\ell^2 + 2R_s\ell)\,, \qquad (17)$$

is the fraction of material in the ϕ-regions.

In indium antimonide the mean free path of electrons at 80° K can be more than 2 μm for samples where impurity scattering is negligible (see Appendix 1), and the ϕ-regions of neighbouring dislocations must be expected to overlap, particularly in the present samples where dislocations were closely spaced in polygon walls. Initially we will assume, however, that this overlap is negligible so that the unmodified Broudy model may be applied.

5.1. Broudy Analysis Assuming no Overlap of ϕ-Regions

A new method of applying Broudy's model to experimental data has been developed which is simpler and more straightforward than that used by the originator.

The Broudy model modifies Read's theory only with respect to scattering, and thus the occupation statistics are not affected. The basic equations 4 and 9 therefore apply, and substituting ρ from equation 4 and R_s from equation 9 in equation 17 gives

$$\phi = K_1\epsilon\,, \qquad (18)$$

where

$$K_1 = \frac{\pi c(N_D - N_A)}{f}\left\{\ell^2 + 2\ell\sqrt{\frac{f}{c\pi(N_D - N_A)}}\right\}. \qquad (19)$$

Substitution of ϕ from equation 18 in equation 14 gives a quadratic equation in ϵ which may be solved to give

$$\epsilon = \frac{2L_1 - (R_0/R_\parallel)M_1 - \sqrt{(R_0/R_\parallel)^2M_1^2 - 4(R_0/R_\parallel)K_1\theta L_1(1-\theta)}}{2L_1^2} \qquad (20)$$

where $L_1 = K_1(1 - \theta) + 1$, and
$M_1 = K_1(1 - \theta^2) + 1$, and the original equation 14 may be rewritten in the form

$$R_0/R_\parallel = \frac{(1 - \epsilon L_1)^2}{(1 - \epsilon M_1)}. \qquad (21)$$

The above equations were used to test the Broudy model in the following way: A value of θ was assumed in order to solve for the other unknowns. It was found, by varying θ, that a real solution of equation 20 could only be obtained with $\theta < 0.1$, and for the following analysis θ was assumed to be 0.05. The significance of this assumption is discussed more fully in section 5.2. A value of the dislocation energy level, $E_C - E_D$, was then chosen and an $f(T)$ curve calculated by Read's "minimum energy" approximation as in section 4.2. Choosing a particular temperature, say 80° K, f (80° K) was read from this calculated curve, and, using also the experimental value of $R_0/R_\parallel$ at 80° K and the mean free path ℓ (80° K) calculated from the experimental electron mobility as described in Appendix 1, ϵ (80° K) was calculated by equation 20. Then equation 5 was used to calculate λ from ϵ (80° K) and f (80° K) and, since it is independent of temperature, this value of λ was used to calculate the whole $\epsilon(T)$ curve from the $f(T)$ curve over the range 80 to 300° K. Finally, using equation 21, $(R_0/R_\parallel)$ was calculated over the whole range of temperature from this $\epsilon(T)$ curve. This $R_0/R_\parallel$ (T) curve is a purely theoretical one, except for the use of $(R_0/R_\parallel)$ (80° K) to obtain λ and the use of the measured electron mobility to obtain the mean free path.

A series of $R_0/R_\parallel$ (T) curves was calculated as described above for a range of energy levels within the forbidden gap, but none of these fitted the experimental points. All the theoretical curves were steeper than the experimental ones, the fit being closest when the dislocation acceptor level was nearest the valence band. Since there was no problem in obtaining a fit on the Read model, the difficulty here must be ascribed to the rapid variation of ϕ with temperature. This variation would be less rapid if neighbouring ϕ-regions overlapped, as was likely in the present samples, and the model was therefore modified to include the degree of overlap expected with polygonised dislocations.

5.2. Modified Broudy Model for Polygonised Dislocation Arrays

Typical arrangements of dislocations in the bent samples are shown in fig. 2. The dislocations lie in polygon walls spaced at about 5 to 10 μm, whilst the separation of dislocations within a wall is 1 to 2 μm. Since the space charge cylinders are probably about 0.5 μm in diameter (for $f \simeq 0.05$) and the mean free path is about 1 to 2 μm, overlap is very likely to occur in the polygon walls, but unlikely between neighbouring walls, and the model shown in fig. 11 was therefore adopted. Here the specimen consists of a

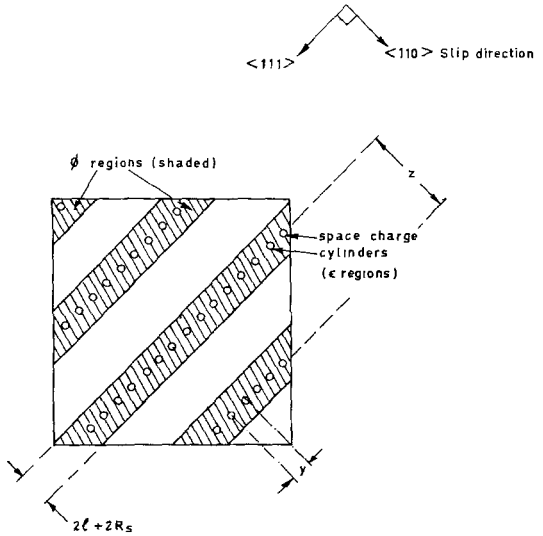

Figure 11 Broudy model modified for samples containing polygonised dislocations.

series of walls of ϕ material, of thickness $(2\ell + 2R_S)$ separated by material of unaltered mobility. There is a row of space-charge cylinders along the centre of each ϕ-wall. This model will be a good approximation if $(2\ell + 2R_S) \gg y$, (see fig. 11) as is expected in most of the present samples when in the extrinsic temperature range. If z is the distance between the centres of neighbouring walls then the fractional area occupied by the $(\phi + \epsilon)$ walls is $(2R_S + 2\ell)/z$, and the volume fraction will be the same. Therefore

$$\phi = 2(R_S + \ell)/z - \epsilon\,,$$
$$= 2(R_S + \ell)\,\rho y - \epsilon\,. \qquad (22)$$

Substituting ρ from equation 4 and R_S from equation 9 we obtain

$$\phi = K_1'\epsilon\,, \qquad (23)$$

where

$$K_1' = \frac{2yc(N_D - N_A)}{f}\left\{\sqrt{\frac{f}{c\pi(N_D - N_A)}} + \ell\right\} - 1. \qquad (24)$$

It is important to note that two unknowns, y and z, have been introduced in place of the one unknown, ρ, and it is therefore necessary to insert the value of y, obtained from the etch-pit spacing in the particular specimen, to carry out the analysis. The value of y rather than that of z is inserted for the following reason: for this analysis it is necessary to leave the dislocation density as an adjustable parameter through which $(\phi + \epsilon)$ at a given temperature may be adjusted. If the value of z were inserted the number of walls per unit volume would be known and $\phi + \epsilon\ (= 2(R_S + \ell)/z)$ would effectively be fixed since $\gg R_S$. However, insertion of y does not predetermine $(\phi + \epsilon)$ since the number of walls per unit volume is still adjustable.

Equation 23 is the counterpart of equation 18 for the no overlap model, and, the analysis was carried out, exactly as in section 5.1, except that K_1' was substituted for K_1 in equation 20 and 21. Fits were obtained between theoretical and experimental $R_0/R_{\|}(T)$ curves as shown in fig. 12 for specimen G5 which gives reasonable agreement for $E_C - E_D = 0.04$ eV. From the value of

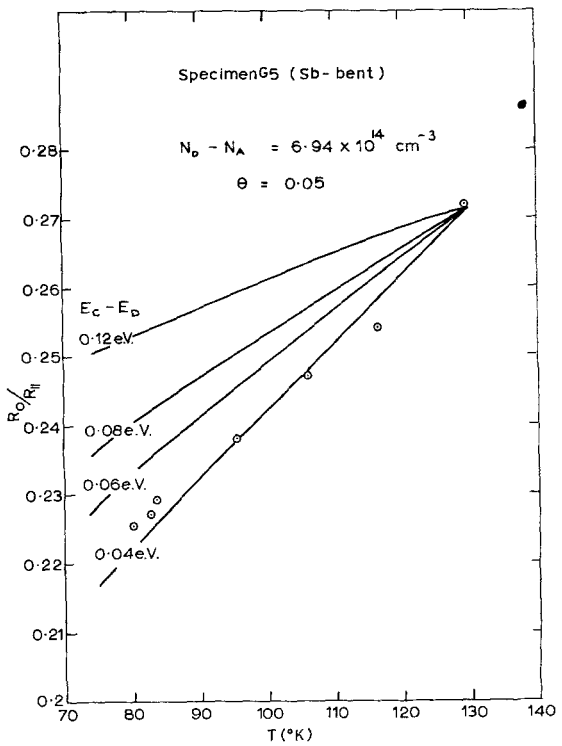

Figure 12 Experimental values of $R_0/R_{\|}$, plotted against temperature, compared with curves calculated on the modified Broudy model for various values of the dislocation energy level.

λ used to obtain this theoretical curve the dislocation density was calculated by equation 6. Table V lists the values of dislocation acceptor level and dislocation density which were obtained in this way for two In-bent and two Sb-bent samples. The derived energy levels for the two In-bent samples agree closely as do those for the two Sb-bent samples and this level scheme

TABLE V Broudy interpretation of $R_0/R_{\parallel}(T)$ measurements

Spec. no.	Excess dislocation type	$E_C - E_D$, eV	Dislocation density, cm^{-2} Calculated	Etch-pit density (butylamine etch)
G6	In	0.06	7.48×10^6	5.82×10^6
G3	In	0.06	3.56×10^7	3.30×10^7
G4	Sb	0.04	4.05×10^6	1.71×10^6
G5	Sb	0.04	3.42×10^7	1.44×10^7

is shown in fig. 13. The calculated dislocation densities are all within a factor of 2.5 of the etch-pit densities.

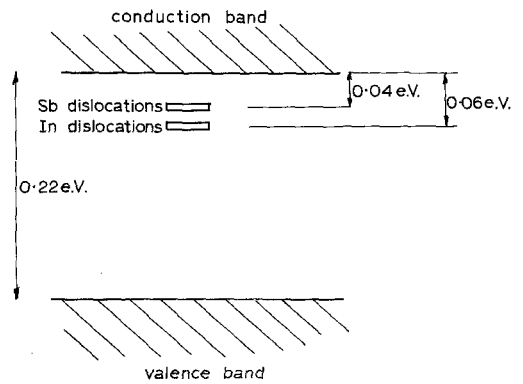

Figure 13 Scheme of dislocation acceptor levels resulting from the modified Broudy analysis.

With the information on the energy levels and dislocation distributions derived above, the conductivity ratios $\sigma_{\parallel}/\sigma_0$ and $\sigma_{\perp}/\sigma_{\parallel}$ at 80° K were obtained from equations 15 and 16 using equation 23 to calculate ϕ and setting θ equal to 0.05 as before. Table VI shows the values of f and ϕ computed for each specimen at 80° K, and compares calculated and experimental values of $\sigma_{\parallel}/\sigma_0$, $\sigma_{\perp}/\sigma_{\parallel}$ (and $R_0/R_{\parallel}$). The agreement for $\sigma_{\parallel}/\sigma_0$ is good, but poor for $\sigma_{\perp}/\sigma_{\parallel}$. However this is not surprising since equation 16 was not rigorously derived by Broudy. One would expect an overestimation of $\sigma_{\perp}/\sigma_{\parallel}$ for large values of $(\epsilon + \phi)$, as Broudy inferred equation 16 from the original Juretschke relation for the Read model, $\sigma_{\perp}/\sigma_{\parallel} = 1/(1 + \epsilon)$, which overestimates $\sigma_{\perp}/\sigma_{\parallel}$ for large ϵ [15].

It was noted in section 5.1 that real solutions of equation 20 could only be obtained with $\theta < 0.1$. The reason for this limitation, which was not mentioned by Broudy, is the limited validity of the models discussed above. The value of θ which is assumed has an effect on the dislocation density which results from the analysis; a high value of θ means that the ϕ-regions are relatively ineffective in increasing the Hall coefficient and consequently a high dislocation density is needed to explain the Hall coefficient change. Above a certain density the dislocations are so closely spaced that the value of ϕ calculated on the assumed model becomes greater than 100%. This maximum dislocation density is thus the limit to the validity of the model* and corresponds to the maximum permissible value of θ, which in this case is 0.1. The value of θ used in the foregoing analysis (0.05) was chosen arbitrarily between the limits of zero and 0.1, but variation of θ within these limits did not alter the resultant energy levels significantly, nor did it change the calculated dislocation density by more than a factor of two. This variation of θ, together with the resultant changes of ϵ and ϕ, produced a change in the calculated values of $\sigma_{\perp}/\sigma_{\parallel}$ and $\sigma_{\parallel}/\sigma_0$, but the latter values were still within experimental error of the measured values.

The above analysis assumed acoustic scattering to be the predominant lattice scattering mechanism. As discussed in section 4.3, it is more likely that polar scattering predominates, and the theory of polar scattering, and of mixed polar and impurity scattering, was therefore developed [20] assuming an energy-independent relaxation time for polar scattering, to obtain expressions for the mean free path when limited by these mechanisms. The mean free path calculated from these expressions was within 15% of the corresponding

TABLE VI Broudy interpretation of measurements at 80° K

Spec. no.	Excess dislocation type	f(80° K)	ϵ(80° K)	ϕ(80° K)	$R_0/R_{\parallel}$ (80° K) Calc.	Exp.	$\sigma_{\parallel}/\sigma_0$(80° K) Calc.	Exp.	$\sigma_{\perp}/\sigma_{\parallel}$(80° K) Calc.	Exp.
G6	In	0.0206	0.05417	0.766	0.262	0.247	0.218	0.217	0.560	0.320
G3	In	0.0351	0.05501	0.5046	0.4911	0.491	0.466	0.450	0.652	0.347
G4	Sb	0.0127	0.01195	0.6145	0.435	0.430	0.400	0.390	0.624	0.472
G5	Sb	0.0252	0.03104	0.8407	0.2225	0.2255	0.171	0.179	0.546	0.299

*This comment applies strictly only to the modified Broudy model (section 5.2); the original model breaks down as soon as overlap occurs.

values for acoustic scattering, and the temperature-dependence was identical. Because of this similarity, a repeat of the above Broudy analysis, using the mean free path for mixed polar and impurity scattering, produced the same energy levels, dislocation densities within a factor of two, and $\sigma_{\perp}/\sigma_0$ values within 10% of those given in tables V and VI.

6. Discussion

6.1. Interpretation of the Changes in Electrical Properties Produced by Plastic Bending

The observed effects of plastic bending on the electrical properties of indium antimonide have been interpreted in terms of the electrical properties of the dislocations introduced, but the possibility of other interpretations will here be discussed. It is first important to note that the above results show clearly that acceptor centres were introduced by the bending, for although the Hall coefficient of *n*-type material can in principle be increased simply by the introduction of low mobility regions within the sample, only the introduction of acceptors can explain the observed conversion of some of the samples from *n* to *p*-type. The possibility that point-defects or impurities rather than dislocations gave rise to these acceptor centres must be considered. The orientation and conditions of deformation were chosen in these experiments to minimise point defect production, and evidence has been presented which shows that the density of dislocations produced by non-primary slip, which might give rise to point defects when interacting with primary dislocations, was very small. The absence of any change in the electrical properties of "control" and "deformed control" samples due to the heat-treatment, rules out the possibility that the electrical changes in the bent samples were due to simple in-duffusion of impurities, but leaves the possibility of impurities being dragged into the sample by the gliding dislocations [21]. Perhaps the strongest indications that the acceptors are associated with the dislocations rather than with any other defect are (i) the anisotropic mobilities in the deformed samples, (ii) the systematic dependence of acceptor concentration on dislocation density as noted in section 4.1, (iii) the fact that analysis of the Hall coefficient results in terms of isolated acceptors would give a different level for each sample, none of these levels corresponding to any known impurity or radiation-induced defect level, and (iv) the large changes in electron mobility in the "perpendicular" samples which would require concentrations of isolated acceptor centres orders of magnitude greater than those indicated by the Hall coefficient results.

6.2. Minority Sign Dislocations

The presence of minority sign dislocations on the primary slip system was noted from the etch-pit measurements (section 3.1) but neglected in the detailed interpretations of the electrical measurements in order to simplify the analyses. However, we here extend the Read theory to accommodate the presence of both In- and Sb-dislocations in the same sample, and analyse the results on this basis so as to ascertain the importance of the minority sign dislocations.

Assuming that each type of dislocation has a discrete energy level, and that both levels lie below the Fermi level in *n*-type material, the two arrays of acceptor centres will have quite independent occupation statistics provided different sign dislocations are not close enough for any mutual electrostatic interaction between the acceptor centres associated with them. If a sample A contains $\rho_{In}{}^{A}$ In-dislocations per cm^2 and $\rho_{Sb}{}^{A}$ Sb-dislocations per cm^2, the fraction of sites occupied being $f_{In}{}^{A}$ and $f_{Sb}{}^{A}$ respectively, then

$$\epsilon^{A} = \frac{f_{In}{}^{A}\rho_{In}{}^{A} + f_{Sb}{}^{A}\rho_{Sb}{}^{A}}{c(N_D - N_A)} . \qquad (25)$$

Suppose a second sample B has a similar initial carrier concentration, and is bent in the opposite sense, then $f_{In}{}^{A} = f_{In}{}^{B}$ $(= f_{In})$ and $f_{Sb}{}^{A} = f_{Sb}{}^{B}$ $(= f_{Sb})$. The selective etching experiments showed that the proportion of minority dislocations was slightly different for the two directions of bend but we will assume a proportion of $\frac{1}{3}$ in both cases. (It will be shown that this value has only a small effect on the results and incorporation of the exact ratios would thus make little difference.) Then

$$\epsilon^{A} = \lambda^{A}(f_{In} + \tfrac{1}{3}f_{Sb}) , \qquad (26)$$

and

$$\epsilon^{B} = \lambda^{B}(\tfrac{1}{3}f_{In} + f_{Sb}) , \qquad (27)$$

where

$$\lambda^{A} = \frac{\rho_{In}{}^{A}}{c(N_D - N_A)} , \qquad (28)$$

and

$$\lambda^{B} = \frac{\rho_{Sb}{}^{B}}{c(N_D - N_A)} . \qquad (29)$$

Note that it is not necessary to make any assumptions about the relative magnitudes of λ^A and λ^B nor for the samples A and B to be bent to equal radii because λ^A and λ^B can be determined independently. Energy levels were then obtained from the temperature-dependence of the Hall coefficient of samples G3 and G5, which fulfil the requirement of having similar initial carrier concentrations, by means of the following extension of the method used in the original Read analysis. Energy levels were assigned to In- and Sb-dislocations and $f_{In}(T)$ and $f_{Sb}(T)$ curves were calculated as before. Then, using equations 26 and 27, experimental values of ϵ^A and ϵ^B at one temperature were used to determine λ^A and λ^B, from which theoretical $\epsilon^A(T)$ and $\epsilon^B(T)$ curves were constructed. Different combinations of energy levels were tried, but the only combination which gave fair agreement for both specimens was $(E_C - E_D)_{In} = 0.06$ eV and $(E_C - E_D)_{Sb} = 0.24$ eV as shown in fig. 14. The values of λ^A and λ^B used to calculate these curves yielded the dislocation densities ρ_{In} and ρ_{Sb} by equations 28 and 29, which are compared with those deduced from etch-pit values in table VII. The discrepancies between theoretical and experimental dislocation densities are approximately the same as in the original Read analysis and the positions of the energy levels have not been altered radically by the above, modified treatment. It is therefore concluded that neglecting minority sign dislocations does not introduce appreciable errors into the results.

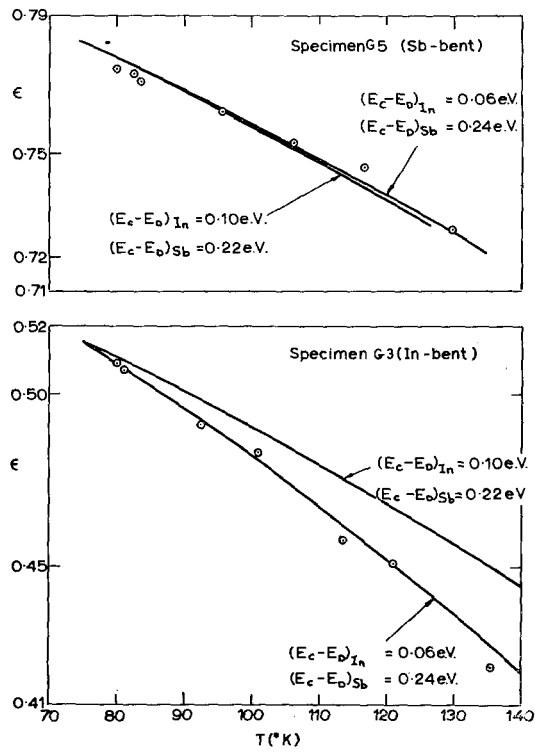

Figure 14 Experimental values of $\epsilon(= 1 - R_0/R_{\parallel})$, plotted against temperature for specimens G5 and G3, compared with curves calculated on the Read model assuming the presence of minority sign dislocations in each sample.

The inclusion of minority dislocations in the Broudy analysis would not be expected to alter the results of that interpretation significantly either, in view of the dominance of the ϕ-regions which are common to both types of dislocation.

6.3. Comparison of the Read and Broudy Dislocation Models

The modification of Read's model suggested by Broudy gives rise to quite different energy level positions and dislocation densities when applied to the present results. Similar, but less dramatic, changes are brought about when this modification is applied to the results of investigations on germanium, and Bell, Birbeck and Willoughby [22] have shown that the difference in acceptor levels suggested by Logan *et al* [13] and Broudy [5] for dislocations in germanium are solely due to the different models used rather than to differences in their measurements. The differences between analyses based on the two models are greater in the case of indium antimonide by virtue of the long mean free path which causes the ϕ-regions to dominate electrical conduction

TABLE VII Read analysis assuming presence of minority dislocations, for dislocation acceptor levels of $(E_C - E_D)_{In} = 0.06$ eV, $(E_C - E_D)_{Sb} = 0.24$ eV

Spec. no.	Excess dislocation type	ρ_{Sb}, cm^{-2} Calculated	Etch-pit	ρ_{In}, cm^{-2} Calculated	Etch-pit
G3	In	5.04×10^7	8.0×10^6	1.51×10^8	2.5×10^7
G5	Sb	1.64×10^8	1.10×10^7	5.46×10^7	3.5×10^6

in the Broudy model. In a typical case the ϕ-regions occupy 76% and the space charge cylinders occupy 5% of the material; furthermore the mobility in the ϕ-regions is necessarily very small for the reasons discussed above. These large ϕ-regions render dislocations very effective in increasing the Hall coefficient in *n*-type material, and consequently the Broudy analysis predicts much smaller dislocation densities than the Read model. Similarly the strong dependence of the mean free path on temperature dominates the temperature-dependence of the Hall coefficient and the Broudy energy level analysis is thus very sensitive to the detailed arrangement of dislocations. An example of this is afforded by the two dislocation arrangements used above, one of which (the polygonised model) gave levels near the conduction band, while in the other (the (no-overlap model) a solution could only be approached with an energy level near the valence band.

To discriminate between the two alternative models discussed here, the results of each analysis must be considered in combination with experimental work on *p*-type material. The main objection to the Read model is the lack of agreement between predicted and experimental dislocation densities. The principal objection to the analysis based on the Broudy model, however, is that it cannot explain the conversion of samples from *n*- to *p*-type as both levels are near the conduction band. Furthermore, recent experiments (Bell and Willoughby [6] and Baitinger *et al* [7] have noted the introduction of acceptor centres after plastic bending of *p*-type material, and Bell and Willoughby have deduced from these results an energy level scheme similar to that in fig. 9. It is therefore concluded that the unmodified Read model gives the more appropriate energy level scheme for dislocations in indium antimonide, but the large discrepancy between predicted and measured densities remains an unsolved problem. It is felt, therefore, that the inclusion of a small degree of non-specular scattering into the basic Read model might achieve a result which gives closer quantitative agreement of dislocation densities while causing little change to the Read scheme of levels. As emphasised by Broudy, his "two-region" model is strictly a first approximation and one would rather expect a smooth change in mobility nearing the dislocation. Furthermore, as discussed above, the limitations of this model force the assumption of what appears to be an unreasonably low mobility in the ϕ-regions. The present situation therefore requires a more rigorous treatment of conduction in material containing a parallel array of insulating cylinders, where the degree of non-specular scattering at the cylinders is a variable parameter, or better still where an attempt is made at a quantitative prediction of the scattering behaviour.

6.4. Comparison with Previous Work

In the preliminary investigation [1] an energy level scheme was suggested in which both acceptor levels were below the centre of the forbidden energy gap but inverted with respect to the present Read scheme. In fact all the results on *n*-type material were in agreement with the present results, and the inverted position of the levels was required to accommodate measurements on a single *p*-type sample, whose behaviour has not been confirmed by a more systematic study of deformed *p*-type material [6]. The consistency of the previous results on *n*-type material is emphasised by fig. 6 in which they lie, within experimental error, on the lines describing the present results.

Previous work on the effect of plastic bending on the electrical properties of indium antimonide [5, 16, 23] has been discussed critically in [1]. In all these investigations the discrepancies between the numbers of acceptors introduced and those predicted on a dangling bond model are greater than those found in the present work. The results of Duga [16] cannot be explained in terms of dislocation acceptors only, for whilst the mobility results can be accommodated with dislocation densities close to those calculated from the bend radii, the Hall coefficient results require dislocation densities higher by two orders of magnitude [1]. This indicates that the Hall coefficient changes were probably dominated by randomly distributed acceptors which produce only small changes in mobility. The results of Gatos *et al* [23] show extremely large effects which are very difficult to understand on any model [1]. The measurements of Broudy [5] show closer agreement with the present results, but no complete analysis was attempted by Broudy in this case because of substantial experimental scatter in the results. In no case was a single slip orientation used for deformation in these previous experiments, and the differences between these studies and the present results could well be due in part to the presence of point defects.

7. Conclusions

(i) Both In- and Sb-dislocations act as acceptor centres in *n*-type material.
(ii) The In-dislocation level lies near the centre of the band gap, while the Sb-level lies near the valence band.

Acknowledgement

Part of this investigation was carried out in the Department of Metallurgy, Imperial College, and the authors are grateful to Professor J. G. Ball for provision of laboratory facilities. The work was supported by a CVD contract and is published by permission of the Ministry of Defence (Navy Department). During the earlier part of the programme one of us (A. F. W. Willoughby) was in receipt of a Beit Fellowship for Scientific Research and later on of an ICI Fellowship.

The authors are grateful to Drs J. B. Mullin, K. F. Hulme, and colleagues at RRE, Malvern who supplied the indium antimonide crystals and took part in many useful discussions.

Appendix 1

Calculation of the Mean Free Path

The Broudy analysis in section 5 requires the calculation of the mean free path in samples where the mobility is limited by mixed scattering. Assuming acoustic scattering to be the predominant lattice scattering mechanism, the following expression, due to Johnson and Whitesell [24], gives the mean free path as a function of carrier energy E, and the degree of impurity scattering, β.

$$\ell(x) = \frac{\ell_A x^2}{x^2 + \beta}, \qquad \text{(A1)}$$

where

$$\ell_A = \frac{3\mu_A}{4q}\sqrt{2\pi m^* kT}$$

and

$$x = E/kT.$$

The average $\bar{\ell}$ over the Maxwellian distribution, is given by

$$N\bar{\ell} = 2\int_0^\infty \ell(E)\,N(E)f(E)\,dE,$$

where

$$N = 2\int_0^\infty N(E)f(E)\,dE$$

is the total number of electrons.

Now, for a non-degenerate electron gas

$$f(E) = A_1 e^{-E/kT},$$

and, for spherical energy surfaces the density of states is given by

$$N(E) = B_1 E^{\frac{1}{2}}.$$

Therefore

$$\bar{\ell} = \frac{\int_0^\infty \ell(x)\,x^{\frac{1}{2}}e^{-x}\,dx}{\int_0^\infty x^{\frac{1}{2}}e^{-x}\,dx} = \frac{2}{\sqrt{\pi}}\int_0^\infty \ell(x)\,x^{\frac{1}{2}}e^{-x}\,dx. \qquad \text{(A2)}$$

TABLE A1 Integral used for calculating the mean free path for acoustic plus impurity scattering

$\beta = \frac{6\mu_A}{\mu_I}$	$I(\beta) = \int_0^\infty \frac{x^{\frac{5}{2}}}{x^2+\beta}e^{-x}\,dx$
0.001	0.8781
0.003	0.8687
0.005	0.8609
0.008	0.8512
0.010	0.8456
0.030	0.8064
0.050	0.7799
0.080	0.7496
0.100	0.7330
0.300	0.6285
0.500	0.5675
0.800	0.5055
1.000	0.4747
3.000	0.3188
5.000	0.2507
8.000	0.1942
10.000	0.1701
30.000	0.07968
50.000	0.05305
80.000	0.03557
100.000	0.02922
300.000	0.01055
500.000	0.006451
800.000	0.004076

TABLE A2

Spec. no.	$N_D - N_A$, cm^{-3}	β(80° K)	$\bar{\ell}$(80° K), cm
G5	6.94×10^{14}	1.5	1.18×10^{-4}
G3	5.68×10^{14}	0.92	1.38×10^{-4}
G6	7.11×10^{13}	0.041	2.23×10^{-4}
G4	1.075×10^{14}	0.016	2.35×10^{-4}

Substituting $\ell(x)$ from equation A1 into equation A2 we obtain

$$\bar{\ell} = \ell_A \frac{2}{\sqrt{\pi}} I(\beta) , \qquad \text{(A3)}$$

where

$$I(\beta) = \int_0^\infty \frac{x^{\frac{5}{2}}}{x^2 + \beta} e^{-x} dx \cdot$$

Values of the integral $I(\beta)$ which was evaluated numerically by computer, are given in table A1. Equation A3 was then used to calculate the mean free path for mixed scattering from the values of β calculated from the temperature-dependence of the carrier mobility (as described in section 4.3) given in table A2, and using for μ_A the measured mobility in samples G6 or G4 where the degree of impurity scattering is very small. Values of $\bar{\ell}$ calculated by this method are listed in table A2.

References

1. R. L. BELL, R. LATKOWSKI, and A. F. W. WILLOUGHBY, *J. Mater. Sci.* **1** (1966) 66.
2. P. HAASEN, *Acta. Met.* **5** (1957) 598.
3. R. L. BELL and A. F. W. WILLOUGHBY, *J. Mater. Sci.* **1** (1966) 219.
4. W. T. READ, *Phil. Mag.* **45** (1954) 775 *ibid* 1119; *ibid* **46** (1955) 111.
5. R. M. BROUDY, *Adv. Phys.* **12** (1963) 135.
6. R. L. BELL and A. F. W. WILLOUGHBY, to be published.
7. U. BAITINGER, J. ARNDT, and D. SCHNEPF, *J. Mater. Sci.* **4** (1969) 396.
8. J. R. PATEL, *J. Appl. Phys.* **29** (1958) 170.
9. E. H. PUTLEY, *Proc. Phys. Soc.* **73** (1959) 280; *ibid* **76** (1960) 802.
10. H. EHRENREICH. *J. Phys. Chem. Solids* **2** (1957) 131; *ibid* **9** (1959) 129.
11. H. C. GATOS and M. C. LAVINE, *J. Electrochem. Soc.* **107** (1960) 427.
12. D. B. HOLT, *J. Phys. Chem. Solids* **23** (1962) 1353.
13. R. A. LOGAN, G. L. PEARSON, and D. A. KLEINMAN, *J. Appl. Phys.* **30** (1959) 885.
14. P. HAASEN and E. SPRINGER, private communication.
15. H. J. JURETSCHKE, R. LANDAUER, and J. A. SWANSON, *J. Appl. Phys.* **27** (1956) 838.
16. J. J. DUGA, *J. Appl. Phys.* **33** (1962) 169.
17. R. T. BATE, R. K. WILLARDSON, and A. C. BEER, *J. Phys. Chem. Solids* **9** (1959) 119.
18. A. H. WILSON, "The Theory of Metals" (Cambridge University Press, 1958).
19. A. C. BEER, J. A. ARMSTRONG, and I. N. GREENBERG, *Phys. Rev.* **107** (1957) 1506.
20. A. F. W. WILLOUGHBY, Ph.D. Thesis (London 1965)
21. A. H. COTTRELL and M. A. JASWON, *Proc. Roy. Soc.* **A199** (1949) 104.
22. R. L. BELL, J. C. H. BIRBECK, and A. F. W. WILLOUGHBY, to be published.
23. H. C. GATOS, M. C. FINN, and M. C. LAVINE, *J. Appl. Phys.* **32** (1961) 1174.
24. V. A. JOHNSON and W. J. WHITESELL, *Phys. Rev.* **89** (1953) 941.

Received and accepted 19 November 1969.